Published by IOP Publishing for Sissa Medialab

Received: *November 3, 2023*
Accepted: *January 29, 2024*
Published: *March 5, 2024*

Topical Workshop on Electronics for Particle Physics
Geremeas, Sardinia, Italy
1–6 October 2023

Compact silicon photonic Mach-Zehnder modulators for high-energy physics

S. Cammarata[a,b,c,*] **F. Palla**[a] **S. Saponara**[b] **F. Di Pasquale**[c] **P. Velha**[a,d] **and S. Faralli**[a,c]

[a] *Istituto Nazionale di Fisica Nucleare, Sezione di Pisa, Largo Bruno Pontecorvo / Edificio C, 56127 Pisa, Italy*
[b] *Dipartimento di Ingegneria dell'Informazione, Università di Pisa, Via Girolamo Caruso 14, 56122 Pisa, Italy*
[c] *Istituto di Intelligenza Meccanica, Scuola Superiore Sant'Anna, Via Giuseppe Moruzzi 1/Area CNR, 56124 Pisa, Italy*
[d] *Dipartimento di Ingegneria e Scienza dell'Informazione, Università di Trento, Via Sommarive 9, 38123 Povo, Italy*

E-mail: simone.cammarata@phd.unipi.it

Abstract: The characterization of compact non-traveling-wave Mach-Zehnder modulators for optical readout in high-energy physics experiments is reported to provide power-efficient alternatives to conventional traveling-wave devices and a more resilient operation compared to ring modulators. Electro-optical small-signal and large-signal measurements showcase the performances of custom NTW-MZMs designed and fabricated in iSiPP50G IMEC's technology in the framework of INFN's FALAPHEL project. Bit-error-rate results demonstrate their potential suitability for optical links up to 25 Gb/s when equipped with either conventional deep-etched or radiation-hardened shallow-etched free-carrier-based phase shifters.

Keywords: Data acquisition concepts; Optical detector readout concepts; Radiation-hard electronics

*Corresponding author.

https://doi.org/10.1088/1748-0221/19/03/C03009

Contents

2024 JINST 19 C03009

1 Introduction

Novel radiation-tolerant optical links are required to handle the foreseen growth in data volumes and radiation intensities expected for the innermost regions of next-generation detectors, e.g., the high-luminosity large-hadron collider (HL-LHC) [1] or the future circular collider (FCC) [2, 3]. For instance, the readout units that will be installed during the Phase II upgrade in all the HL-LHC experiments [4] are based on the Low-power Gigabit Transceiver (lpGBT) and the Versatile Transceiver Plus (VTRx+), which will respectively implement on-detector data serialization and electro-optical (EO) conversion to realize bi-directional communication links with data rates up to 10.24 Gb/s [5, 6]. Regarding the up-link transmission, the VTRx+ module harnesses directly-modulated vertical-cavity surface-emitting lasers (VCSELs), which are known to be extremely susceptible to performance degradation as radiation levels rise. They are currently capable of tolerate only up to $1 \cdot 10^{15}$ cm^{-2} 1-MeV equivalent neutron fluences [4], preventing VTRx+ systems to be directly installed in the innermost regions of the HL-LHC detectors [7]. Therefore, data generated in those layers are initially transmitted via bulky bandwidth-limited electrical cables to dedicated service shells characterized by radiation levels appropriate for long-term VTRx+ operation [4]. A qualitative architecture of these data links is shown in figure 1.

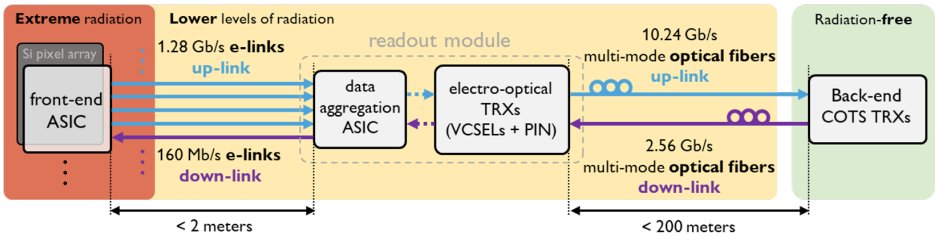

Figure 1. Architecture of currently deployed optical links in high-energy physics detectors [8].

The presence of electrical links (e-links) restricts the possibility to scale up data-rates and together improve power consumption and material budget. In this context, the pressing need to find alternative technologies for the evolution of radiation-hard optical links has led to the evaluation of silicon photonics (SiPh) [9]. SiPh components have indeed recently demonstrated impressive radiation tolerance thanks to the application of proper design hardening techniques and annealing procedures [10–15]. Although being still under deeper investigation regarding the stability of radiation

effects and efficacy of the implemented countermeasures, fully-integrated SiPh-based transceivers (TRXs) prototypes are already under development to provide next-generation readout systems for high-energy physics (HEP) detectors [16–20]. In comparison to existing optoelectronic modules, SiPh also presents a distinct advantage in terms of transmission capabilities. SiPh can deliver transmission bandwidths that exceed 50 Gb/s per lane while maintaining low power consumption [21]. In addition, it can bring higher levels of integration on detector by providing inherent possibilities for data aggregation, e.g., through wavelength- or polarization-based multiplexing, which do not require to expand the count of physically installed optical fibers.

In the implementation of SiPh-based transmitters, the selection of the EO modulating devices becomes critical in addressing system-level requirements. Standard open-access SiPh platforms typically allow to implement high-speed intensity modulation via Mach-Zehnder (MZMs) or ring modulators (RMs) equipped with depletion-driven PN-junction phase shifters. While RMs offer compact sizes, low-power operation and straightforward wavelength division multiplexing (WDM) capabilities, their resonance is highly sensitive to temperature and process fluctuations, often requiring power-intensive wavelength-locking mechanisms to ensure their correct functioning [22]. On the other hand, MZMs are optically broadband and do not typically require strict stabilization against environmental changes. Nonetheless, when using MZMs, long phase shifting sections are required to achieve reasonable modulated extinction ratios with small driving voltages. They thus easily end up to have millimeter-scale rectilinear lengths which impose careful radio-frequency (RF) design to embed the phase shifters in transmission lines (TLs) where the modulating electrical waveform co-propagate with the optical wave to efficiently impress the data modulation [23]. This traveling-wave (TW) design translates in the need for on-chip termination resistors to avoid RF reflection-induced inter-symbol interference. Both static and dynamic power dissipation take place in these terminations and make TW-MZMs less power-efficient than RMs [24, 25]. To provide a more compact and low-power interferometric modulator version to be used in HEP, we will report in this work the experimental characterization of non-traveling-wave MZMs (NTW-MZMs) designed to be used without on-chip termination impedance to reduce power consumption.

2 Device design

The power consumption and footprint reduction in MZMs can be achieved by shrinking the overall size of the electrodes which contact the phase shifters. Traveling-wave effects indeed arise only when the wavelength of the driving signal becomes a non-negligible fraction of the physical device length [26]. Hence, in a more compact component RF reflection effects will start to be noticeable only at relatively higher driving frequencies. However, an extension of the lumped-element condition by simply shortening a rectilinear MZM is not convenient since phase shift performances will be reduced at the same time. To decouple RF size and optical length, we propose to layout the MZMs with meandered phase shifting sections contacted via interdigitated electrodes, as shown in figure 2. This allows to fold two arms with 1.5 mm-long doped waveguides into an approximate 500 µm × 500 µm area, considering also the required bond-pads. To give a fair comparison, an analogous rectilinear MZM with the same doped length would have a footprint of about 500 µm × 2 mm while typical RMs occupy around 400 µm × 150 µm footprint, including bond-pads for the active PN-junction and the unavoidable thermal heater for resonance control. The overall structure of the device design can be checked in [27], while here we will focus in the characterization of two different versions of the same

2024 JINST 19 C03009

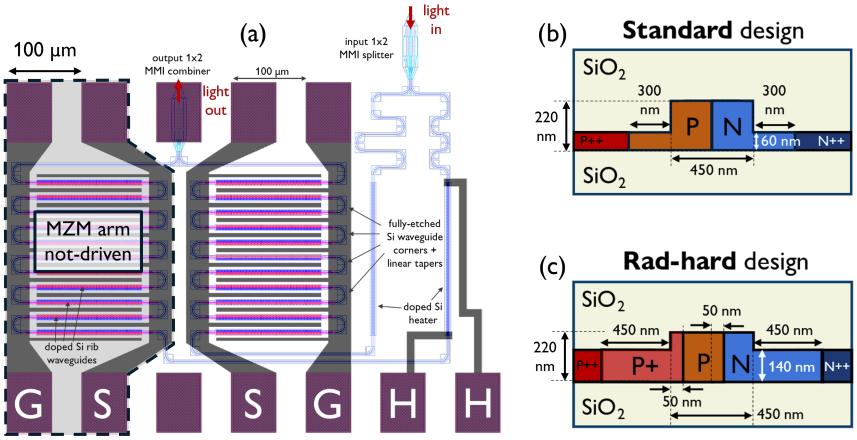

Figure 2. (a) Overview of the proposed folded MZM with meandered phase shifters, together with the (b) standard and (c) radiation-hardened waveguide cross-sections implemented with the same layout. Acronyms: ground (G), signal (S), heater (H), low core P-type doping (P), low core N-type doping (N), high core P-type doping (P+), slab P-type doping (P++), slab N-type doping (N++).

folded MZM (FMZM). As indicated in figure 2, FMZMs with conventional and radiation-hardened phase shifters have been included in the same photonic integrated circuit (PIC). The standard design employs deep-etched slabs with a PN-junction formed with the lowest doping levels available in iSiPP50G technology. In the second version, radiation hardening is implemented by introducing both shallow-etched waveguide slabs as well as an additional P-doped area with higher doping concentration in the region where radiation-induced degradation is expected to take place [10]. While the position of the active PN junction was nominally set in the middle of the waveguide in the standard design, it was shifted by 50 nm towards the cathode region in the rad-hard version. This was done to ensure a comparable small-signal depletion capacitance between the two devices. The P-type doping reinforcement was indeed extended by 50 nm inside the rib waveguide core to ensure proper coverage of the radiation-sensitive slab. Instead, the offset of the slab doping implants from the waveguide core edge has been respectively set to 300 nm and 450 nm in the conventional and the radiation-hardened designs to avoid excessive propagation losses because of the different optical confinements in the two waveguide types.

3 Experimental characterization

Device characterizations have been performed in both direct-current (DC) and radio-frequency (RF) conditions at die-level with optical and electrical probes to single-out real device performances by avoiding the parasitic contributions introduced by packaging. In general, only a single arm for each FMZM was driven with electrical signals, while the other one was kept to a constant 0 V bias during all the experiments. A DC EO spectral characterization was first carried out for each device with the same setup and methods described in [9]. The acquired spectra are reported in figure 3, together with the length-normalized phase shift and modulation efficiency, i.e., the so-called $V_\pi l_\pi$ product, for both PN junction types. While the FMZM with standard design presents a minimum $V_\pi l_\pi$ of 1.8 V cm, the radiation-hardened one is limited to 3 V cm. By subtracting the reference optical spectrum from

2024 JINST 19 C03009

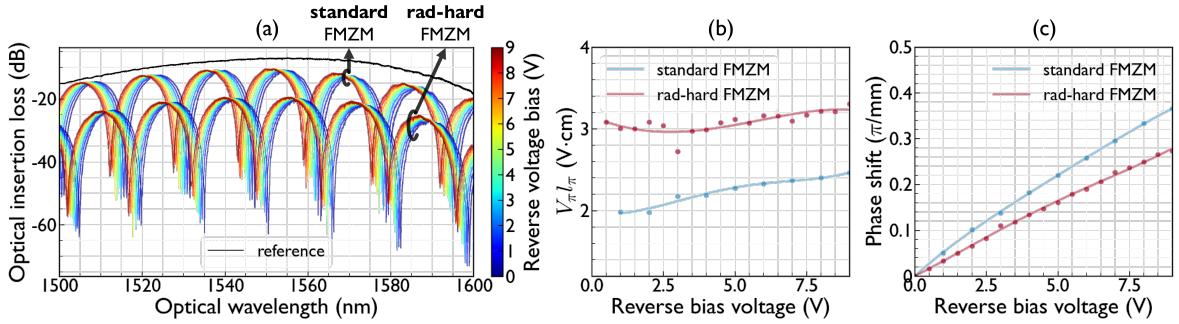

Figure 3. Electro-optical DC spectral characterization. (a) Acquired optical spectra as a function of reverse voltage bias. Length-normalized (b) half-wave voltage $V_\pi l_\pi$ and (c) phase shift for each FMZM design.

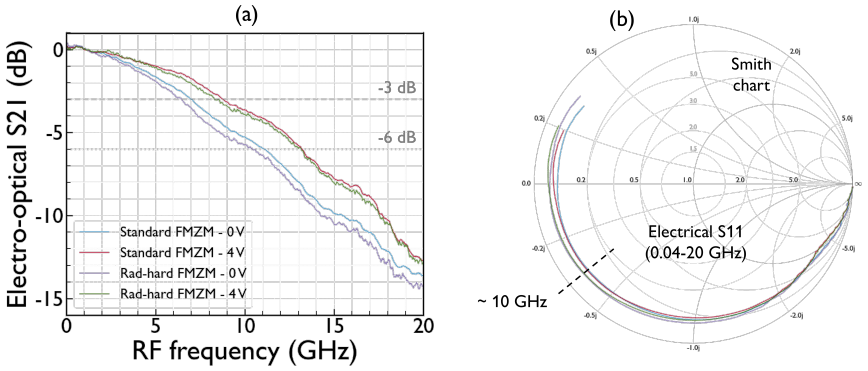

Figure 4. Electro-optical large-signal FMZMs characterization. (a) EO transmission S21 parameter and (b) electrical reflection S11 parameter for 0 V and 4 V reverse voltage biases.

the device measurements to separate the contributions of fiber-to-PIC coupling and test setup losses, optical propagation losses of approximately 15 dB/cm and 60 dB/cm near 1550 nm were extracted for the standard and rad-hard PN junction designs, respectively. The higher $V_\pi l_\pi$ and the substantial loss increase in the rad-hard case can be attributed to the lower optical confinement intrinsic to shallow-etched rib waveguides and the consequent larger mode overlap with free carriers.

Electro-optical RF small-signal and large-signal characterizations have been conducted with the same procedure described in [27]. Small-signal EO -3 dB transmission bandwidths for both devices were measured in the range 6.5 GHz to 9 GHz varying the PN junctions' reverse bias from 0 V to 4 V. As shown in figure 4, the symmetry in this result between both devices confirms that the P+ doping addition does not alter the main PN junction capacitance.

Figure 5 reports the EO bit-error-rate (BER) measurements as a function of optical received power and bit-rate, together with the corresponding eye diagrams. They where conducted applying an effective peak-to-peak 4.4 V voltage[1] with 4 V bias voltage to both devices. Even in the presence of gradual eye closures compatible with the measured EO bandwidths, both FMZMs achieve BER ratings well below KP4 forward error correction (FEC) threshold up to 25 Gbit/s. Instead, at 30 Gbit/s,

[1]The measured peak-to-peak voltage on the oscilloscope's internal 50 Ω load is around 2.2 V, as also shown in figure 5. However, because of the highly-reflective capacitive load presented by the device due to the absence of an on-chip RF termination, as reported in figure 4(b), the effective voltage applied on the modulator's access pads can be considered, at worst, twice the value measured on the oscilloscope.

2024 JINST 19 C03009

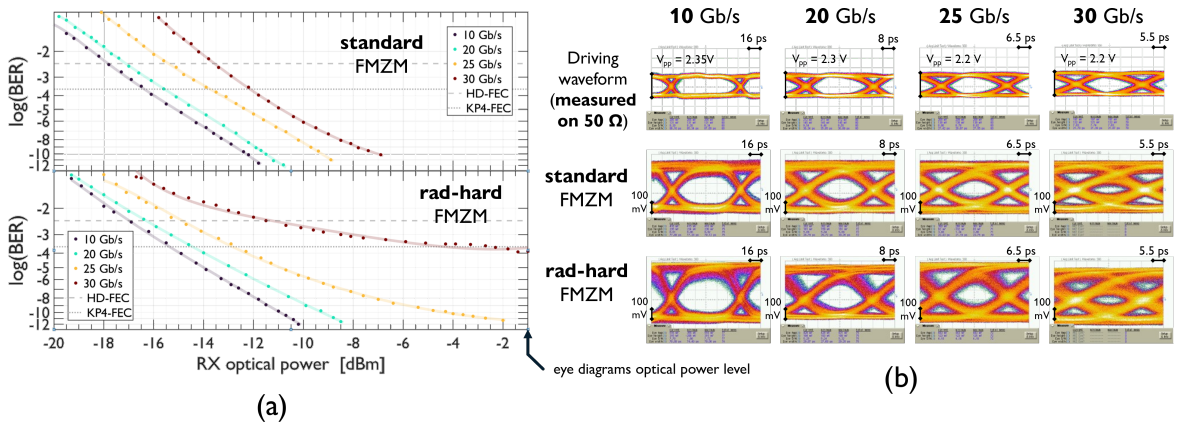

Figure 5. Electro-optical large-signal FMZMs characterization. (a) Bit-error-rate (BER) measurement as a function of optical received power and bit-rate. (b) Corresponding eye diagrams of the driving voltage applied to modulators' pads and the received modulated signals for both FMZM designs in the same conditions of optical power impinging on the photo-receiver.

the FMZM with conventional design guarantees smooth operability, while the rad-hard one, in the same conditions, presents a BER floor which does not go below the KP4 FEC threshold even when increasing the received optical power. This behavior is attributed to the relative difference in modulation efficiencies between the two devices.

4 Conclusions

Compact NTW-MZMs can be regarded as competitive alternatives to resonant RMs, offering the advantages of interferometric devices, such as reduced sensitivity to temperature fluctuations, with smaller power and footprint impact than conventional TW-MZMs. By folding phase shifters in the MZMs arms following a meandered pattern, it was possible to gain a 4-fold footprint reduction with respect to rectilinear TW-MZMs with the same phase shifter lengths. To evaluate their performance metrics and extend the SiPh components portfolio for HEP applications, two FMZMs have been experimentally characterized. One device was designed with conservative deep-etched phase shifters with conventional PN junction doping levels. The second was instead equipped with radiation-hardened-by-design phase shifting sections, employing both shallow-etched waveguides and a boosted doping level on the anode portion of the phase shifter.

The proposed FMZMs resulted in less than 10 GHz EO modulations bandwidths and achieved almost error-free NRZ transmissions up to 25 Gbit/s for both devices with 4.4 V peak-to-peak voltage driving. It should be remarked that these performances were recorded in a 50 Ω testing environment. One of the bandwidth limits of lumped-element modulators is indeed the resistance-capacitance (RC) time constant associated with charging/discharging the PN junction device depletion capacitance [28]. Therefore, a substantial bandwidth improvement can be obtained by co-designing an electronic driver with low-output impedance and higher current sourcing/sinking strengths in order to decrease RC time constants. Of course, this might translate in more power consumption on the electronics side [29]. Focused studies might be needed to find the optimal trade-off between bandwidth and power consumption. Nevertheless, the presented performances can still prove valuable in HEP detector systems where ultra-high bit rates per single device are sometimes unnecessary, as this would otherwise require more intensive forms of electronic data aggregation on detectors.

2024 JINST 19 C03009

Acknowledgments

This work was supported by INFN-funded projects FALAPHEL, PHOS4BRAIN and ISHTAR (jointly funded by UniPi).

References

[1] G. Apollinari et al. eds., *High-luminosity large hadron collider (HL-LHC): Technical design report v. 0.1*, CERN-2017-007-M (2017) [DOI:10.23731/CYRM-2017-004].

[2] FCC collaboration, *FCC-ee: The Lepton Collider: Future Circular Collider Conceptual Design Report Volume 2*, *Eur. Phys. J. ST* **228** (2019) 261.

[3] FCC collaboration, *FCC-hh: The Hadron Collider: Future Circular Collider Conceptual Design Report Volume 3*, *Eur. Phys. J. ST* **228** (2019) 755.

[4] CMS collaboration, *The Phase-2 Upgrade of the CMS Tracker*, CERN-LHCC-2017-009, CMS-TDR-014 (2017) [DOI:10.17181/CERN.QZ28.FLHW].

[5] J. Troska et al., *The VTRx+, an optical link module for data transmission at HL-LHC*, *PoS* **TWEPP-17** (2017) 048.

[6] P. Moreira and S. Kulis, *Radiation-hard ASICs for data transmission and clock distribution in High Energy Physics*, *Nucl. Instrum. Meth. A* **1053** (2023) 168364.

[7] J. Troska, F. Vasey and A. Weidberg, *Radiation tolerant optoelectronics for high energy physics*, *Nucl. Instrum. Meth. A* **1052** (2023) 168208.

[8] T. Prousalidi et al., *Towards optical data transmission for high energy physics using silicon photonics*, 2022 *JINST* **17** C05004.

[9] S. Cammarata et al., *Silicon photonic devices for optical data readout in high-energy physics detectors*, *Nucl. Instrum. Meth. A* **1045** (2023) 167576.

[10] M. Zeiler et al., *Radiation Damage in Silicon Photonic Mach-Zehnder Modulators and Photodiodes*, *IEEE Trans. Nucl. Sci.* **64** (2017) 2794.

[11] A. Kraxner et al., *Investigation of the Influence of Temperature and Annealing on the Radiation Hardness of Silicon Mach-Zehnder Modulators*, *IEEE Trans. Nucl. Sci.* **65** (2018) 1624.

[12] A. Kraxner et al., *Radiation tolerance enhancement of silicon photonics for HEP applications*, *PoS* **TWEPP2018** (2019) 150.

[13] M. Lalović et al., *Ionizing Radiation Effects in Silicon Photonics Modulators*, *IEEE Trans. Nucl. Sci.* **69** (2022) 1521.

[14] I. Reghioua et al., *Radiation Effects on Si-Photonics-Integrated Passive Devices: Postirradiation Measurements*, *IEEE Trans. Nucl. Sci.* **70** (2023) 1973.

[15] G.N. Tzintzarov et al., *Direct Measurement of Total-Ionizing-Dose-Induced Phase Shifts in Commercially Available, Integrated Silicon-Photonic Waveguides*, *IEEE Trans. Nucl. Sci.* **70** (2023) 2116.

[16] Y. Zhang et al., *Key building blocks of a silicon photonic integrated transmitter for future detector instrumentation*, 2019 *JINST* **14** P08021.

[17] S. Cammarata et al., *Design and Performance Evaluation of Multi-Gb/s Silicon Photonics Transmitters for High Energy Physics*, *Energies* **13** (2020) 3569.

[18] G. Ciarpi et al., *Design and Characterization of 10 Gb/s and 1 Grad TID-Tolerant Optical Modulator Driver*, *IEEE Trans. Circuits. Syst. I Regul. Pap.* **69** (2022) 3177.

2024 JINST 19 C03009

[19] C. Scarcella et al., *System development of silicon photonics links for CERN experiments and accelerators*, 2023 *JINST* **18** C03002.

[20] T. Prousalidi et al., *System Development of Radiation-Tolerant Silicon Photonics Transceivers for High Energy Physics Applications*, *IEEE Trans. Nucl. Sci.* **70** (2023) 2373.

[21] M. Pantouvaki et al., *Active Components for 50 Gb/s NRZ-OOK Optical Interconnects in a Silicon Photonics Platform*, *J. Lightw. Technol.* **35** (2017) 631.

[22] S. Agarwal et al., *Wavelength Locking of a Si Ring Modulator Using an Integrated Drop-Port OMA Monitoring Circuit*, *IEEE J. Solid-State Circuits* **51** (2016) 2328.

[23] D. Patel et al., *Design, analysis, and transmission system performance of a 41 GHz silicon photonic modulator*, *Opt. Express* **23** (2015) 14263.

[24] A. Rahim et al., *Taking silicon photonics modulators to a higher performance level: state-of-the-art and a review of new technologies*, *Adv. Photonics* **3** (2021) 024003.

[25] B. Murray, C. Antony, G. Talli and P.D. Townsend, *Predistortion for High-Speed Lumped Silicon Photonic Mach-Zehnder Modulators*, *IEEE Photonics J.* **14** (2022) 1.

[26] S. Sharif Azadeh et al., *Power-efficient lumped-element meandered silicon Mach-Zehnder modulators*, *Proc. SPIE* **11285** (2020) 112850C.

[27] S. Cammarata et al., *30 Gb/s NRZ Transmission with Lumped-Element Silicon Photonic Mach-Zehnder Modulator*, in the proceedings of the *2022 IEEE Photonics Conference (IPC)*, Vancouver, BC, Canada (2022), p. 1–2 [DOI:10.1109/ipc53466.2022.9975756].

[28] J. Witzens, *High-Speed Silicon Photonics Modulators*, *Proc. IEEE* **106** (2018) 2158.

[29] S. Zhou et al., *Optimization of PAM-4 transmitters based on lumped silicon photonic MZMs for high-speed short-reach optical links*, *Opt. Express* **25** (2017) 4312.